



**HAL**  
open science

# Lifting the cover of the cauldron: Convection in hot planets

Y. Ricard, S. Labrosse, F. Dubuffet

► **To cite this version:**

Y. Ricard, S. Labrosse, F. Dubuffet. Lifting the cover of the cauldron: Convection in hot planets. *Geochemistry, Geophysics, Geosystems*, 2014, 15 (12), pp.4617-4630. 10.1002/2014GC005556 . hal-02046717

**HAL Id: hal-02046717**

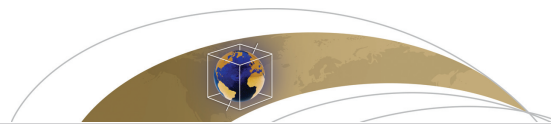
**<https://hal.science/hal-02046717>**

Submitted on 20 Dec 2021

**HAL** is a multi-disciplinary open access archive for the deposit and dissemination of scientific research documents, whether they are published or not. The documents may come from teaching and research institutions in France or abroad, or from public or private research centers.

L'archive ouverte pluridisciplinaire **HAL**, est destinée au dépôt et à la diffusion de documents scientifiques de niveau recherche, publiés ou non, émanant des établissements d'enseignement et de recherche français ou étrangers, des laboratoires publics ou privés.

Copyright

RESEARCH ARTICLE **Lifting the cover of the cauldron: Convection in hot planets**

10.1002/2014GC005556

Yanick Ricard<sup>1</sup>, Stéphane Labrosse<sup>1</sup>, and Fabien Dubuffet<sup>1</sup><sup>1</sup>Laboratoire de Géologie de Lyon, École Normale Supérieure de Lyon, Université Lyon-1, Université de Lyon, CNRS UMR5276, Lyon, France**Key Points:**

- Convection and erosion can be strongly coupled on young planets
- A heat pipe mechanism can cool a young planet very rapidly
- Free slip conditions may not be appropriate in mantle convection models

**Correspondence to:**Y. Ricard,  
Ricard@ens-lyon.fr**Citation:**Ricard, Y., S. Labrosse, and F. Dubuffet (2014), Lifting the cover of the cauldron: Convection in hot planets, *Geochem. Geophys. Geosyst.*, 15, 4617–4630, doi:10.1002/2014GC005556.

Received 22 AUG 2014

Accepted 26 OCT 2014

Accepted article online 17 NOV 2014

Published online 2 DEC 2014

**Abstract** Convection models of planetary mantles do not usually include a specific treatment of near-surface dynamics. In all situations where surface dynamics is faster than internal dynamics, the lateral transport of material at the surface forbids the construction of a topography that could balance the internal convective stresses. This is the case if intense erosion erases the topography highs and fills in the depressions or if magma is transported through the lithosphere and spreads at the surface at large distances. In these cases, the usual boundary condition of numerical simulations, that the vertical velocity cancels at the surface should be replaced by a condition where the vertical flux on top of the convective mantle equilibrates that allowed by the surface dynamics. We show that this new boundary condition leads to the direct transport of heat to the surface and changes the internal convection that evolves toward a heat-pipe pattern. We discuss the transition between this extreme situation where heat is transported to the surface to the usual situation where heat diffuses through the lithosphere. This mechanism is much more efficient to cool a planet and might be the major cooling mechanism of young planets. Even the modest effect of material transport by erosion on Earth is not without effect on mantle convection and should affect the heat flow budget of our planet.

**1. Introduction**

Shortly after they form, telluric planets are very hot as they have to evacuate the tremendous heat provided by the decay of short period radioactive elements [Carlson and Langmuir, 2000], by the surface impacts [Tonks and Melosh, 1993], and by the release of potential energy due to core-mantle segregation [Ricard et al., 2009; Šrámek et al., 2010]. Young planets are also potentially heated by tidal dissipation [Robuchon et al., 2010] as it is the case for Io, one of the Jovian satellites [Peale et al., 1979]. In these very situations, O'Reilly and Davies [1981] proposed that heat might be advected through the surface by isolated vents [see also Turcotte, 1989]. The transport of heat by volcanism in the early Earth has also recently been discussed by Moore and Webb [2013]. This situation was mimicked by Monnereau and Dubuffet [2002] with numerical simulations of convection with perfectly "open" surface boundary conditions (e.g., a zero vertical derivative of the vertical velocity).

Heat extraction entirely by transport across the surface, for example during explosive volcanism, is an extreme situation. A huge heat flow is also extracted during magmatic flood events: heat is radiated and diffused out through a frozen boundary layer orders of magnitude thinner than the lithosphere so that heat appears directly delivered at the surface. Various mechanisms of planetary resurfacing can also lead to an enhanced cooling of a planet. Chemical and mechanical erosion, by removing material above thermal doming and depositing sediments in the topographic lows above thermal downwellings also favor the cooling of the planetary interiors.

The advective transport of heat through the surface occurs every time the vertical surface velocity  $v_h$  differs from the vertical material velocity  $v_z$  by a quantity  $v_e$ , which represents the erosion/deposition velocity, the eruption velocity (the eruption mass flow divided by the mantle density), or accounts for the lateral speeding of magma (Figure 1). The solution of the heat equation with a moving boundary condition is straightforward and indicates that the temperature is perturbed over a depth  $\kappa/v_e$  ( $\kappa$  is thermal diffusivity). This length has to be compared with the thickness  $d$  of the thermal lithosphere that controls the diffusion of heat. When these two lengths become comparable, erosion transports as much heat as would have been diffused out through a lithosphere with no erosion. For Earth, ( $d \approx 120$  km,  $\kappa \approx 10^{-6}$  m<sup>2</sup> s<sup>-1</sup>) this occurs as

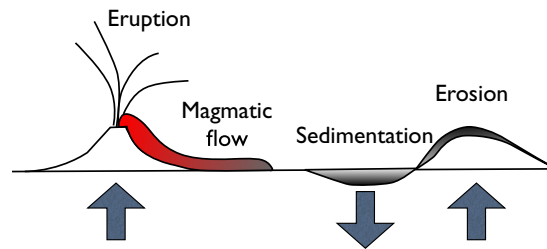


**Figure 1.** There are various situations where the shallow surface dynamics implies the existence of a vertical velocity at depth and therefore the transport of heat through the reference level of the surface.

[e.g., Biot and Odé, 1965]. However, the processes that couple the internal and surface dynamics with the surface heat flow have never been discussed in a general framework. The majority of mantle convection studies imposed a zero vertical velocity at the surface considered with a fixed altitude and do not account for a specific surface dynamics. In this paper, we review and discuss the boundary conditions applied at the surface of convection codes and we proposed a new set of conditions.

soon as  $v_e \sim 0.4 \text{ mm yr}^{-1}$ . This is not a very large value and for any stronger erosion or deposition rates, the heat flux is going to be affected by surface processes.

At small scale, the fact that erosion and deformation are coupled has been emphasized for a long time, for example in the case of diapir formation

## 2. Surface Boundary Conditions on Top of a Convective Fluid

In a laboratory experiment performed by confining a fluid between two plates, the no-slip condition (the fluid velocity cancels at the contact with the plates) is certainly appropriate. When the fluid is not confined between fixed horizontal boundaries, various levels of approximation are routinely implemented.

Due to convective stresses, the free surface of a liquid is slightly deformed, to a “depth”  $z = -h(x, y, t)$ , much smaller than the fluid thickness, and the normal  $\mathbf{n}$  to the surface is not strictly vertical [see also Ricard, 2007]. The topography  $h(x, y, t)$  is often called in the geophysical literature “dynamic” topography (i.e., not related to the Moho undulations). The free surface condition imposes that the normal components of the total stress tensor vanish,

$$\underline{\sigma}(x, y, h(x, y, t), t) \cdot \mathbf{n} = 0. \tag{1}$$

This vectorial condition provides three dynamical conditions, but introduces the unknown quantity  $h$ . The hydrostatic balance provides first-order estimates of deviatoric stress  $\underline{\tau} = \mathcal{O}(\rho g \alpha \Delta T d)$  and topography  $h = \mathcal{O}(\alpha \Delta T d)$  ( $\alpha$  is the coefficient of thermal expansion,  $\rho$  the density,  $\Delta T$  the temperature jump across the top thermal boundary of average thickness  $d$ ). The condition (1) is therefore often replaced by

$$\underline{\sigma}(x, y, 0, t) \cdot \mathbf{n} + \rho \mathbf{g} \cdot \mathbf{n} h(x, y, t) = 0 \tag{2}$$

within an error of order  $(\alpha \Delta T)^2$ , as estimated by linearizing (1) with respect to  $h$ . Furthermore, the angle of the normal to the vertical is of order  $\alpha \Delta T d / L$  where  $L$  is the horizontal wavelength of convection, and it can be safely neglected (at least at long wavelength when  $L \gg d$ ), so that the free surface conditions can be written as

$$\begin{aligned} \sigma_{zz}(x, y, 0, t) &= -\rho g h(x, y, t), \\ \tau_{zx}(x, y, 0, t) &= \tau_{zy}(x, y, 0, t) = 0. \end{aligned} \tag{3}$$

This provides a zero shear condition at  $z = 0$  for the tangential stresses  $\tau_{zx}$  and  $\tau_{zy}$ ; the small topography  $h$  is controlled by the surface vertical velocity and its weight imposes in turn the normal stress  $\sigma_{zz}$ .

This set of equations is not yet sufficient since  $h$  is unknown. A last condition is provided by the kinematic definition of the topography. If we call  $\mathbf{u}_h$  the horizontal component of the velocity of the surface and  $v_h$  its vertical velocity, the evolution of the topography is given by

$$\frac{\partial h}{\partial t} + \mathbf{u}_h \cdot \nabla h = v_h. \tag{4}$$

Two more approximations are often introduced; first the horizontal gradient of dynamic topography is supposed small enough than it can be neglected, second the vertical surface velocity  $v_h$  is identified with the vertical velocity  $v_z(x, y, 0, t)$  so that the evolution of the topography  $h$  becomes

$$\frac{\partial h(x, y, t)}{\partial t} = v_z(x, y, 0, t). \quad (5)$$

Even in the forms (3)–(5), this leads to numerical problems. The viscous time of relaxation of a free surface, which also controls the postglacial rebound, is only of a few thousand years at long wavelengths. To avoid numerical instabilities, codes implementing the conditions (3)–(5), require either a specific approach [see *Kaus et al.*, 2010] or a time stepping of only a few hundred years which makes a convection simulation over a geological time of billion years extremely expensive. In most numerical codes used to simulate mantle convection, free-slip boundary conditions are used

$$\begin{aligned} v_z(x, y, 0, t) &= 0, \\ \tau_{xz}(x, y, 0, t) &= \tau_{yz}(x, y, 0, t) = 0. \end{aligned} \quad (6)$$

The resulting normal stress is then used to estimate the topography generated by the convective flow [*Richards and Hager*, 1984]. Internal compositional interfaces can be treated in a similar manner if they are only weakly deformable (i.e., when their intrinsic density jumps are much larger than the thermal density variations). This is the case for the core-mantle boundary.

Various authors have tried to overcome the series of approximations that lead to the free-slip conditions. *Kaus et al.* [2010] or *Duretz et al.* [2011] solved for the time dependence of the topography (5) using a finite element formalism for the Navier-Stokes equation and taking into account the advection of the interfaces by a first order correction in time of the loading terms. *Schmeling et al.* [2008] proposed another approximation consisting in adding a thin layer with zero density and weak viscosity in between what should be the real free surface and a fixed layer where a no-slip boundary is imposed, the so-called “sticky-air” approach [see also *Cramer et al.*, 2012a, 2012b].

There are various geological situations where free-slip, (6), and free surface conditions, (1) and (4), lead to different results. One case was studied by *Zhong et al.* [1996]. For short wavelength structures and for rapid events (e.g., for a localized thermal anomaly impinging the Earth’s surface), the viscous stresses transmitted by the fluid interior can be shielded by the elastic strength of the lithosphere, the time for topographic equilibration becomes comparable to the time scale of internal convective processes, and the slope of the topography itself may become large. In this case the precise computation of a history-dependent topography is necessary. This is also true in the modeling of slab dynamics where a free surface boundary condition (1) leads to a satisfactory simulation of one-sided subduction, and of slab bending and unbending [*Schmeling et al.*, 2008; *Cramer et al.*, 2012a, 2012b]. In the case of classical free-slip conditions (6), a dripping instability is instead obtained.

### 3. Boundary Conditions for a Fast Surface Dynamics

#### 3.1. New Mechanical Boundary Conditions

Even assuming that the surface topography remains small compared to the convection wavelengths, and readjusts so rapidly compared to the convection time scale that  $\partial h / \partial t = 0$ , the identification of the material velocity with the surface velocity is a major assumption that has not been really discussed in the framework of mantle convection. In lithospheric studies of subduction dynamics, however, through numerical [*Gerya and Stöckhert*, 2006; *Kaus et al.*, 2008] or analog models [*Chemenda et al.*, 1995] it is known that erosion can change drastically the internal dynamics. The same is true in collision zones where erosion is a driving mechanism of mountain building by decreasing the resisting stress that controls the large scale convergent velocities [*Avouac and Burov*, 1996; *Iaffaldano et al.*, 2011].

The velocity  $v_z(x, y, 0, t)$  at the reference level  $z = 0$  (which is the quantity really used in all Eulerian fluid mechanic simulations, i.e., using variables defined on fixed positions) differs from the vertical velocity of the topography  $v_h(x, y, h, t)$  because of the erosion velocity  $v_e(x, y, h, t)$

$$v_z(x, y, 0, t) = v_h(x, y, h, t) - v_e(x, y, h, t) \quad (7)$$

In the case of erosion, the erosion velocity is related to a horizontal transport away from the topographic highs in the direction of the topography lows and is often represented by a diffusion term [*Culling*, 1963; *Kirkby*, 1971; *Kaus et al.*, 2008] so that

$$v_e = \nabla \cdot \mathbf{J} \text{ with } \mathbf{J} = -D_e \nabla h. \tag{8}$$

The exact value of the erodability,  $D_e$ , depends a lot on the morphological settings, on the topographic slope, and increases with the precipitation rate and the down-system distance [Armitage *et al.*, 2011]. The diffusion coefficients of erosion deduced empirically from geological observations range over several decades with values  $D_e = 10^{-6} \text{ m}^2\text{s}^{-1}$  to  $D_e = 10^{-3} \text{ m}^2\text{s}^{-1}$  over mountainous areas [Flemings and Jordan, 1989; Fernandes and Dietrich, 1997; Avouac and Burov, 1996]. These values yield denudation rates of  $0.7 \mu\text{m yr}^{-1}$ – $0.7 \text{ mm yr}^{-1}$  for a 300 km wide topography with 2000 m of relief. In an active orogen and with a climate prone to extreme rainfall events (e.g., in Taiwan) 10 times larger denudation rates are observed [Dadson *et al.*, 2003].

In the case of a spreading magma, the lateral flow can also be computed with a simple model of gravity current [Huppert, 1982] and the lateral flow is of order

$$\mathbf{J} = -D_m \nabla h = -\frac{\rho g h^3}{3\eta_m} \nabla h \tag{9}$$

where  $\eta_m$  is the magma viscosity. The equivalent nonlinear diffusivity  $D_m$  varies a lot according to the magma viscosity ( $1$ ,  $10^6$ , and  $10^9 \text{ m}^2\text{s}^{-1}$  for a dry siliceous melt, a wet siliceous melt, and an oceanic spreading ridge basalt with  $\eta_m = 10^{10}$ ,  $10^4$ ,  $10 \text{ Pa s}$ , respectively and  $h = 100 \text{ m}$ ).

To illustrate the effects of erosion on the convective planform, we assume that the topography is at steady state,  $v_h(x, y, h, t) = 0$ . In this case, the vertical velocity at the Eulerian top surface,  $v_z(x, y, 0, t)$ , just balances the quantity of material that is removed by erosion and by lateral spreading,  $v_e(x, y, 0, t)$ . Defining  $D = D_e + D_m$  as the total coefficient of topographic “diffusion,” the mechanical boundary conditions at the surface are simply

$$\sigma_{zz}(x, y, 0, t) = -\rho g h(x, y, t), \tag{10}$$

$$v_z(x, y, 0, t) = \nabla \cdot (D \nabla h), \tag{11}$$

$$\tau_{xz}(x, y, 0, t) = \tau_{yz}(x, y, 0, t) = 0. \tag{12}$$

### 3.2. Two-Dimensional Mechanical Boundary Conditions

Although the implementation of (10)–(12) is not difficult in 3-D, we will restrict our analysis to the 2-D incompressible Newtonian case (with viscosity  $\eta$ ). We neglect the effects of elasticity which are not expected to be important at large scale, although the interaction between bending stresses and topography may not be negligible locally [Zhong *et al.*, 1996; Kaus and Becker, 2007]. In this case, using the stream function  $\psi$ , the velocity becomes

$$\mathbf{v} = \left( -\frac{\partial \psi}{\partial z}, \frac{\partial \psi}{\partial x} \right), \tag{13}$$

and the fact that the shear stress vanishes (12) is expressed as usual by

$$\frac{\partial^2 \psi}{\partial z^2} = \frac{\partial^2 \psi}{\partial x^2}. \tag{14}$$

The boundary condition (11) is simply

$$\psi = D \frac{\partial h}{\partial x}. \tag{15}$$

The x derivative of (10) becomes after some algebra,

$$3\eta \frac{\partial^3 \psi}{\partial^2 x \partial z} + \eta \frac{\partial^3 \psi}{\partial^3 z} + 4 \frac{\partial^2 \psi}{\partial x \partial z} \frac{\partial \eta}{\partial x} = -\rho g \frac{\partial h}{\partial x}. \tag{16}$$

The topography  $h$  can be eliminated from these two previous equations to obtain

$$3 \frac{\partial^3 \psi}{\partial^2 x \partial z} + \frac{\partial^3 \psi}{\partial^3 z} + 4 \frac{\partial^2 \psi}{\partial x \partial z} \frac{\partial \ln \eta}{\partial x} + R \psi = 0, \tag{17}$$

where we define the topographic resistance,  $R$ , as

$$R \equiv \frac{\rho g H^3}{\eta D} \tag{18}$$

and where the lengths  $x$  and  $z$  are made non dimensional by normalizing them by the depth of the convection layer  $H$ . Notice that in (17) and (18), the viscosity is expressed at the surface, and although it may be variable laterally, its variations are likely opposite to those of the topography diffusion  $D$  (which varies like  $1/\eta$  in (9)), and we assume that  $\eta D$ , and therefore  $R$ , can be considered as constants. The dimensionless number  $R$  is formally a Rayleigh number, ratio of the advective time of convection to the diffusion time of the topography. The Rayleigh number is classically

$$Ra \equiv \frac{\alpha \rho g \Delta T H^3}{\kappa \eta} = R \alpha \Delta T \frac{D}{\kappa} \tag{19}$$

where  $\Delta T$  is the temperature forcing and  $\kappa$  the thermal diffusivity). The equations (14) and (17) applied at the surface of the convective domain ( $z = 0$ ) constitute our new set of mechanical boundary conditions.

In the limiting case where the topography has an infinite resistance (see (10)),  $R \rightarrow +\infty$ ,  $\psi(x, 0) = 0$  which implies according to (13) that  $v_z = 0$ . The usual free-slip boundary conditions are recovered and the top boundary condition is "closed." On the contrary when  $R \rightarrow 0$ , the topography cannot be maintained, the normal stress  $\sigma_{zz}$  is zero, the top boundary condition is "open." This last boundary condition has been used by Monnereau and Dubuffet [2002] to simulate convection in the mantle of Jupiter's moon Io (they also used a zero horizontal velocity,  $\partial\psi/\partial z = 0$ , rather than a zero shear stress (14), which leads to the simplification of (17) on the form  $\partial^3\psi/\partial z^3 = 0$ ). The boundary condition (17) allows the continuous transition from the condition  $v_z = 0$  to the condition  $\sigma_{zz} = 0$  that we will call "closed" and "open" conditions.

Notice that in an experimental setup using fluids with strongly temperature dependent viscosity, interpreting  $\eta$  (in the Rayleigh definition, (19)) as the viscosity of the bulk and  $\eta_m$  (in the topographic resistance, see (9)) as the viscosity of the hot near surface upwellings, leads to  $R = 3(\eta_m/\eta)(H/h)^3 \sim 3(\eta_m/\eta)/(\alpha\Delta T)^3$ . As  $\alpha\Delta T \ll 1$ ,  $R$  is generally very large and the free-slip "closed" condition is satisfied in most common experiments. It is only when the viscosity ratio  $\eta_m/\eta$  between the hot upwellings and the average bulk becomes comparable with, or smaller than  $(\alpha\Delta T)^3$  that low resistance numbers can be obtained. This is the case for a planet where magma is much less viscous than the mantle (typically for a silicate planet  $\eta_m = 10 - 10^{10}$  Pa s and  $\eta \approx 10^{21}$  Pa s while  $(\alpha\Delta T)^3 \approx 10^{-6}$ ) or where erosion is very intense.

### 3.3. Thermal Boundary Conditions

In a convection code we also need to prescribe the boundary conditions for the temperature. We consider  $z$  upward so that erosion (removal of material) corresponds to a positive  $v_z$ . We have seen that near the surface, erosion imposes a thermal boundary layer of thickness  $\kappa/v_z$ . When  $v_z$  is small enough, this boundary is larger than the gridsize  $\Delta z$  of our code, it remains numerically well resolved and we implement an imposed surface temperature  $T_0$ . The same condition is also applied in the case of material deposition  $v_z < 0$ ,

$$T = T_0 \quad \text{when} \quad v_z(x, 0) \leq \frac{\kappa}{\Delta z}, \tag{20}$$

On the contrary, when the vertical velocity at the surface is large, we consider that the temperature is exactly the temperature upstream and use

$$\frac{\partial T}{\partial z} = 0 \quad \text{when} \quad v_z(x, 0) \geq \frac{\kappa}{\Delta z}. \tag{21}$$

All the downward flow through the surface corresponds to material that has lost all his excess heat, but the material that reaches the surface carries its temperature at depth.

The surface heat flux is classically characterized by a Nusselt number which is the ratio of the heat flow effectively transported to the diffusive flow in the absence of convection. In our situation, the heat can be carried out by diffusion across a thermal boundary layer (the usual term  $-k\partial T/\partial z$  where  $k$  is the thermal conductivity) but also by direct transport through the surface (the term  $\rho C_p v_z (T - T_0)$  where  $C_p$  is heat capacity). As we intend to discuss our models both in the case of erosion and of magma transport, we do not consider the latent heat effects. The effective heat capacity should be increased by a latent heat in the

case of magma. Scaled in term of Rayleigh and resistance numbers the difference between sensible and total heat is not of prime order.

It may seem surprising that the boundary conditions (20) and (21) are functions of the gridsize  $\Delta z$  but this is physically reasonable. Consider a planet where heat is released in some places through a thick lithosphere and in other places, by emplacement of lava traps. The former heat release is “conducted,” the later “advected.” However if we were able to describe in the same numerical code the tens of kilometer thick lithosphere and the centimeter scale of the cooling top layer of the lava, all the heat will just appear conducted. The difference of scale between a lithosphere thickness and a lava frozen lid or an eroded layer is so large that distinguishing diffusion from transport suffers in fact no ambiguity. We checked in our numerical experiments that the convection patterns are totally independent of the gridsize  $\Delta z$ . The ratio of diffused to advected heat flow at the surface is very slightly decreasing with the gridsize which has no impact on our results.

#### 4. Numerical Simulations

We implement a finite volume numerical model to solve the convection equations in the Boussinesq approximation and Cartesian geometry. We use a stream function formulation for the equations of motion with a direct implicit inversion method [Schubert *et al.*, 2001]. The heat equation is solved by an Alternating Direction Implicit (ADI) scheme [Peaceman and Rachford, 1955]. The stream function and the temperature field are described by a second-order approximation in space. The simulation are performed in a box with aspect ratio of three with a minimum of  $200 \times 600$  grid points. We use a centered scheme for the advection of temperature which is only stable for grid Peclet number lower than 2 (practically lower than  $\sim 20$ ) [Dubuffet *et al.*, 2000]. As we increase the Rayleigh number, we increase the number of grid points to maintain this stability condition. For  $Ra \sim 10^7$  we use  $500 \times 1500$  grid points. Velocity boundary conditions are free-slip at the bottom and along the sides. On top, a first row of ghost points is used to enforce conditions (14), (20) and (21), while an additional row farther out is necessary to enforce (10). The Rayleigh number is defined in the basal heating case using the temperature difference between the bottom uniform temperature and the top reference temperature of the downwellings. Notice that because the upwellings can directly deliver the hot internal temperature to the surface, the local surface temperature can be much larger than the reference top temperature, and sometimes close to the bottom temperature.

##### 4.1. Basal Heating With Uniform Viscosity

In a first set of numerical experiments we use a uniform viscosity in the internal fluid, (and therefore  $\partial\eta/\partial x = 0$  in the boundary condition (10)) and no internal heating. The parameter  $R$  controls the level of surface opening and we first discuss calculations with a Rayleigh number equal to  $10^6$ . Figure 2 depicts snapshots of the temperature field at statistical steady state for various resistance numbers  $R$ . The same color table is used for the different plots. Down to  $R \approx 10^5$ , the style of convection is very similar to the usual free-slip convection. The gradual opening of the surface by decreasing the resistance  $R$  (from top to bottom of Figure 2), leads to a strong cooling of the fluid, to the progressive reduction of the thickness of the top boundary layer and to the formation of intense hot plumes. The dominant wavelength of the flow also increases with the gradual opening of the upper boundary. When  $R = 0$  (bottom), the basal heat is directly delivered to the surface by narrow hot plumes and no cold thermal boundary layer is present beneath the surface. Similar patterns were obtained by [Monnereau and Dubuffet, 2002] although the fact that we impose a zero shear stress instead of a zero horizontal velocity makes the convection pattern more time dependent.

Figure 3 shows the average temperature computed for various Rayleigh numbers (from  $10^3$  to  $10^7$ ) and resistance numbers  $R$ . For large resistance numbers (i.e., the black,  $R = 3 \times 10^5$ , and red,  $R = 10^5$  curves), the average temperature is close to  $1/2$ , the classical Rayleigh-Bénard value. Decreasing  $R$  or increasing  $Ra$  eases the transport of heat to the surface and decreases the average temperature. When the resistance number reaches 0, except for a few hotspots with temperature close to the basal temperature, the rest of the fluid is passive and its temperature is close to the surface temperature (cyan). Those who have tried to warm up a pea soup should have noticed this peculiar mode of convection, totally inefficient to warm the bulk of the soup.

In Figure 4, we depict the total Nusselt number, sum of advective and diffusive terms. The total Nusselt number is comprised between the Nusselt number of the “closed” case ( $R = 3 \times 10^5$ , black) and that of the “open” case ( $R = 0$ , cyan). These two limiting cases obey a scaling law of the form  $Nu = aRa^b$  with the same

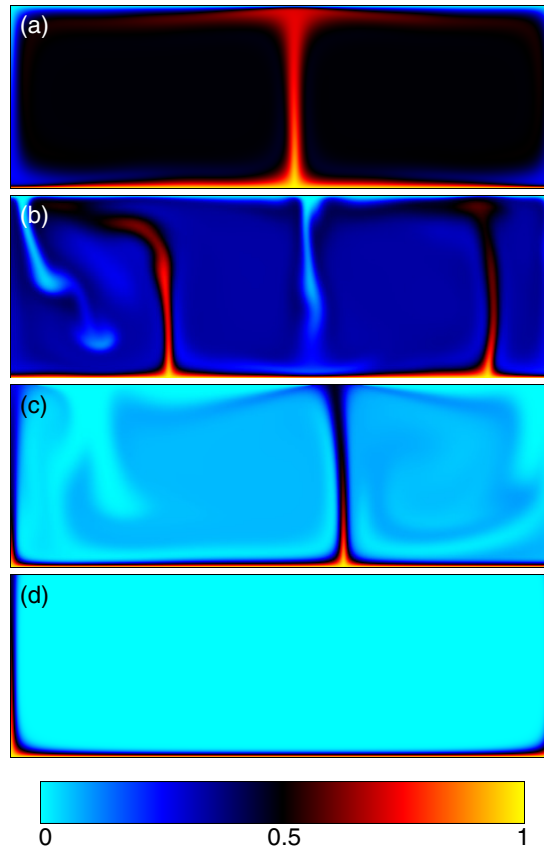


**Figure 2.** Temperature pattern in a convecting box of aspect ratio 3, heated from below, when the top boundary condition is progressively opened ( $R=10^5, 10^4, 10^3, 0$ , from Figures 2a–2d,  $Ra=10^6$ ). The same color table is used for the different plots. Notice the strong cooling of the medium when the surface is progressively opened with the bulk of the fluid at  $T \approx 1/2$  (black, for  $R=10^5$ ) to  $T \approx 0$  (cyan, for  $R=0$ ).

is present across which the temperature decreases by  $\Delta T = T_{max} - T_0$  (see Figure 2d). Through this layer, heat is injected by diffusion then transported to the surface by a thermal plume of width  $\delta$  and velocity  $v$ . The surface heat flow  $\rho C_p \langle v \Delta T \rangle$  is therefore of order  $\rho C_p v \Delta T \delta / H$  and the Nusselt number is thus

$$Nu_o = \frac{\rho C_p \langle v \Delta T \rangle}{k \Delta T / H} \propto v \frac{\delta}{\kappa}. \quad (24)$$

As the system has a negligible kinetic energy (infinite Prandtl number approximation), the mechanical power of the buoyancy forces must be equal to that of the resisting viscous forces. This is expressed by

$$(\alpha \rho \Delta T) g H \delta v \propto (\eta \frac{v}{H}) H v. \quad (25)$$

The thickness  $\delta$  is itself a function of the time during which the bottom boundary thickens by diffusion

$$\delta \propto \sqrt{\frac{\kappa H}{v}} \quad (26)$$

From (24), (25) and (26), we get for the “open” case

$$Nu_o = a Ra^{1/3}, \quad (27)$$

where, using the data of Figure 4, we obtain numerically  $a = 0.36$ . The exponent is the same for the “open” and “closed” cases but there is an enhancement by 60% of the heat flow delivered with “open” conditions compared to the “closed” case (22).

exponent  $b \sim 1/3$  but with a different factor  $a$ , the “open” case leading to a  $\sim 60\%$  higher heat flow. For a given Rayleigh number  $Ra$ , the advected heat flow decreases with  $R$  while the conducted heat flow increases with  $R$ . The transition between the two limiting cases occurs roughly when  $Ra \sim 100R$ .

#### 4.2. Scaling Laws for Basal Heating

In the case of purely basal heating with “closed” boundary conditions, the variation of the surface heat flux with the Rayleigh number can be obtained from analytical boundary layer theory of finite amplitude. For example, *Turcotte and Schubert* [1982] propose that the Nusselt number  $Nu_c$  ( $c$  stands for “closed” surface conditions or infinite  $R$ ) is

$$Nu_c = 0.22 Ra^{1/3}. \quad (22)$$

This relation is rather well satisfied by numerical models and experiments with slight variations in the prefactor and exponent that we do not need to discuss in this paper. Our simulations with a large  $R$  agree with this expression. The average temperature of the fluid is simply

$$\bar{T}_c = \frac{1}{2}. \quad (23)$$

The same type of scaling analysis can be done for the case of “open” surface conditions. A bottom boundary layer of thickness  $\delta$

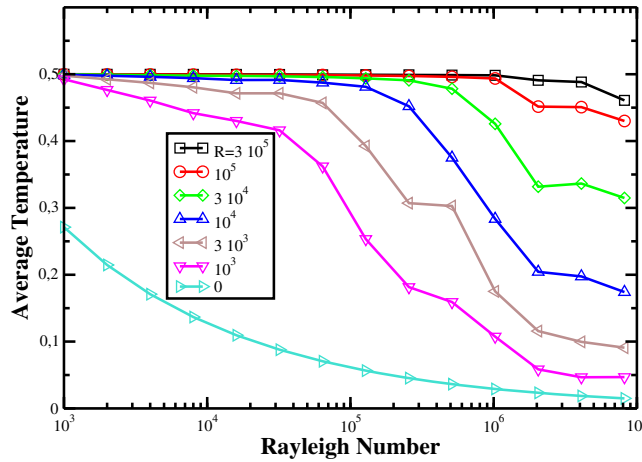


**Figure 3.** Average temperature as a function of the Rayleigh number for different resistance numbers  $R$  (aspect ratio 3, basal heating only). When  $R$  is large (e.g., the black lines for  $R=3 \times 10^5$ ), the average temperature is close to 0.5. The opening of the surface, leads to the strong decrease of the average temperature.

The average dimensionless temperature is zero everywhere except in a thin layer of width  $\delta$  across which the temperature increases from 0 to  $\Delta T$ . The average normalized temperature should therefore be of order

$$\bar{T}_o \propto \frac{\delta}{H} \propto \frac{1}{Nu_o}. \quad (28)$$

The numerical fit (cyan in Figure 3) gives

$$\bar{T}_o = 2.7Ra^{-1/3}, \quad (29)$$

in close agreement with the analytical estimates (with (27) and  $a = 0.36$ ).

Figure 4 shows that the transition between the “closed” and the “open” situations occurs between  $10R \leq Ra \leq 100R$ . The fact that the transition occurs at constant  $Ra / R$  is easy to understand. According to equation (26), the typical velocity is  $v_c \propto \kappa H / \delta^2$ . The typical velocity of erosion above a hot plume is

$$v_e \propto D \frac{\partial^2 h}{\partial x^2} \propto \frac{Dh}{\delta^2} \propto \frac{D\alpha\Delta TH}{\delta^2}. \quad (30)$$

The transition between the “closed” and the “open” situations occurs therefore when  $v_e$  and  $v_c$  become commensurable which occurs when  $\kappa H / \delta^2 \propto D\alpha\Delta TH / \delta^2$  or  $Ra \propto R$ . According to Figure 4, the lithosphere opens when the erosion velocity is larger than 10 times the typical convective velocity.

### 4.3. Internal Heating With Uniform Viscosity

Planetary mantles are largely heated from within, either by radioactivity or tidal deformation, like for example in the case of Io. Moreover, secular cooling is mathematically equivalent to a volumetric heat source [Krishnamurti, 1968]. In the case of convection driven by internal heating only, the Rayleigh number is defined by

$$Ra_i \equiv \frac{\alpha\rho^2gPH^5}{\eta\kappa k}, \quad (31)$$

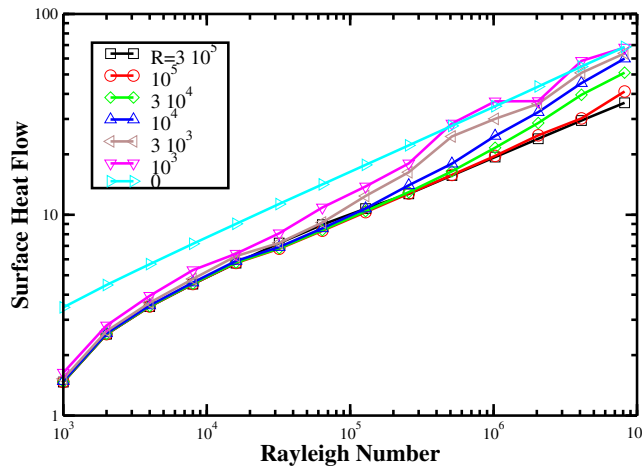


**Figure 4.** Nusselt number as a function of Rayleigh number for different resistance numbers  $R$  (aspect ratio 3, basal heating only). For  $R=3 \times 10^5$ , the surface boundary condition is indiscernible from a free-slip condition in the range of Rayleigh numbers under investigation. For  $R=0$  the top surface is totally “open.” A low  $R$  number eases the transport of heat to the surface by advection and increases the heat flow with respect to the “closed” case by ~60%.

where  $P$  is the rate of heat production per unit mass. Figure 5 depicts the temperature fields for various resistance numbers ( $R=10^6, 10^3, 10^2, 10$  in Figures 5a–5d, respectively), similarly to Figure 2 for the basally heated case. All cases have the same value for the Rayleigh number,  $Ra_i=10^6$ . A different color table is used for the different plots, with the temperature varying between 0 (cyan) and  $T_{max}$  (yellow), the value of  $T_{max}$  being indicated in each plot. The gradual opening of the surface by decreasing the

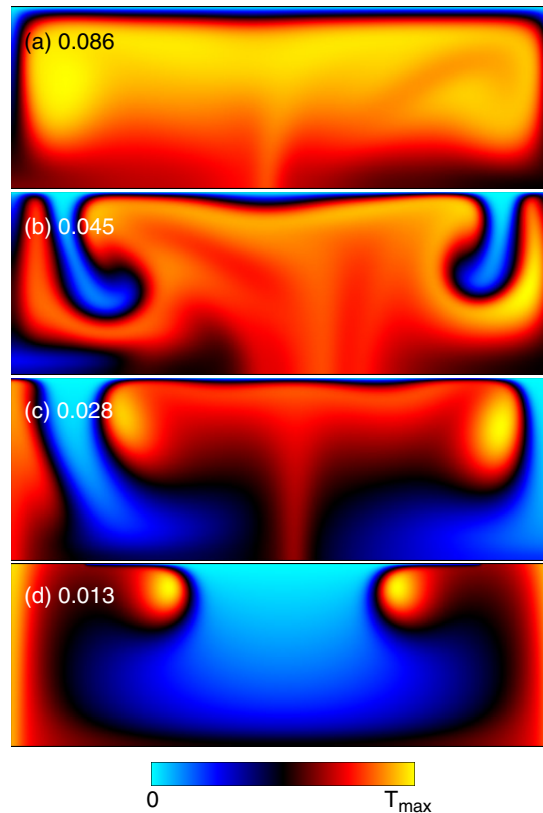


**Figure 5.** Snapshots of the temperature field in a convecting box of aspect ratio 3, heated from within, when the top boundary condition is progressively opened ( $R = 10^6, 10^3, 10^2, 10$  from Figures 5a–5d,  $Ra_i = 10^5$ ). The color scale is between 0 and  $T_{max}$  reported in each plot. The medium is strongly cooling when the surface is progressively opened. Notice that for a very low topographic resistance (Figure 5d), hot plumes are formed although the fluid is only internally heated.

surface leads to a stronger power law dependance of order  $-1/2$  (cyan) in agreement with [Monneréau and Dubuffet, 2002]. The transition between the two regimes occurs also when the Rayleigh number is 100–1000 times the resistance number.

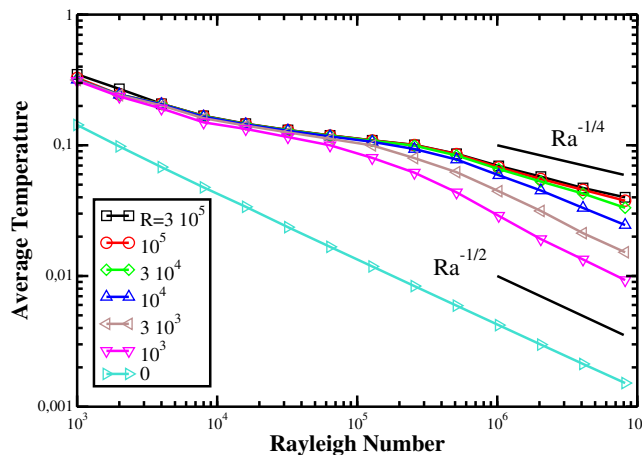


**Figure 6.** Average temperature in a convecting box of aspect ratio 3, heated from within, as a function of the internal Rayleigh and resistance numbers. The slope of the average temperature versus Rayleigh number relation changes from  $\propto Ra_i^{-1/4}$  to  $\propto Ra_i^{-1/2}$  as the topographic resistance is lowered.

resistance  $R$  leads again to a strong cooling of the fluid: the maximum temperature decreases by close to an order of magnitude. When  $R$  decreases, the localized downwellings become larger and larger, until the bulk of the fluid is cold and passively sinking (Figure 5d). On the contrary, the bulk of the fluid is hot and passively rising in the usual closed convection with internal heating (Figure 5a), while hot plumes form in the open situation (Figure 5d). This peculiar mode of convection where hot plumes are formed in the absence of basal heating was first observed in Monneréau and Dubuffet [2002] for the case  $R = 0$ .

The average temperature is depicted in Figure 6 as a function of  $Ra$  and  $R$ . The Rayleigh number dependance of the average temperature changes with the resistance number. At large  $R$ , the temperature-Rayleigh number relation is a power law with exponent  $-1/4$ . The opening of the sur-

#### 4.4. Scaling Laws for Internal Heating

In a “closed” box, the average temperature  $\bar{T}$  normalized by  $\rho PH^2/2k$  scales as  $Ra_i^{-1/4}$  [Turcotte and Schubert, 1982; Parmentier et al., 1994]:

$$\theta_c \equiv \frac{2k\bar{T}}{\rho PH^2} = 2.98 Ra_i^{-1/4}. \quad (32)$$

The internal temperature can also be simply estimated when the top surface is open. In this case there is no thermal boundary layer, the only lengthscale is  $H$  and the heat flow advected across the top surface balances the internal heat production

$$\rho C_p v \Delta T H \propto \rho P H^2. \tag{33}$$

Similarly to (25), the balance of the rates of work and dissipation is

$$\alpha \rho \Delta T g H^2 v \propto \left(\eta \frac{v}{H}\right) H v \tag{34}$$

Because of the absence of lengthscale, the average temperature is simply  $\bar{T}_c \propto \Delta T$ . From these expressions of average temperature, heat budget and energy balance (33) and (34), we get for the “open” case

$$\theta_o = a R a_i^{-1/2}. \tag{35}$$

and we find numerically  $a = 5.7$ . The normalized internal temperature decreases much more strongly with  $R a_i$  than with the usual “closed” boundary condition. Like in the bottom heated case, the transition between “closed” and “open” cases occurs when the convective and erosional velocities become comparable, which happens at constant  $R a / R$ .

### 5. Effects of Depth and Temperature-Dependent Viscosity Variations

In the case of the formation of narrow vents carrying heat to the surface, the viscosity should be strongly laterally variable, notably because of temperature variations. We therefore explore a few cases assuming a mantle viscosity of the form  $\eta = \eta_0 \exp(c_1 z - c_2 T)$ . In Figure 7, we consider the case of basal heating only. The left column depicts the temperature field, the right one, the viscosity. The Rayleigh number based on  $\eta_0$  is  $10^6$  and the resistance number  $R = 10^3$ , like Figure 2c. We choose  $c_1$  and  $c_2$ , so that the viscosity increases by a factor 10 with depth and decreases by a factor 1,  $10^2$ ,  $10^4$  with temperature, from top to bottom row. The resulting minimum and maximum viscosities are indicated in the right plots (e.g., in Figure 2d, the viscosity varies between  $0.1 \eta_0$  and  $7.4 \eta_0$ ). In the first row, the viscosity variations due to temperature in the reference conductive case, balance those due to pressure and this case is roughly comparable to Figure 2c. The downwellings become somewhat more localized as the dependence of viscosity with temperature is increased (compare Figure 2a with Figure 2e). When the viscosity of the bottom layer becomes very low, secondary convection starts inside this layer as can be seen in the emerging hot instability of (Figure 2e), and solitary waves are traveling along the hot conduits. However, the convection pattern and the average

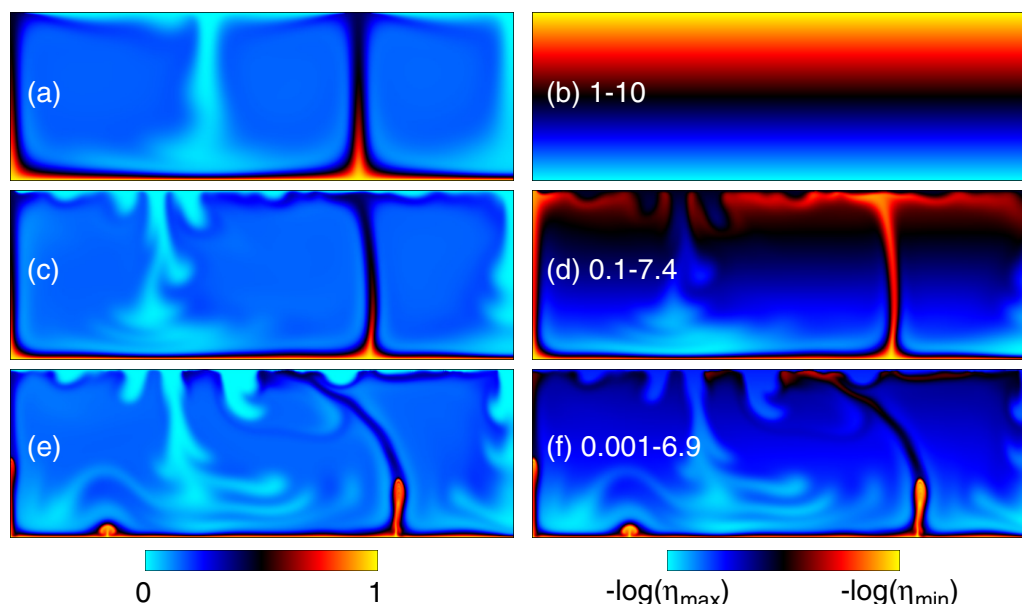


**Figure 7.** Snapshots of (left) temperature and (right) viscosity in a convecting box of aspect ratio 3 heated from below with temperature and depth-dependent viscosity. The Rayleigh number based on the surface viscosity at  $T = 0$  is  $10^6$  in all simulations and the resistance is  $R = 10^3$ . The temperature varies from  $T = 0$  to  $T = 1$  on the left. The viscosity increases by a factor 10 with depth and decreases exponentially with temperature. The resulting minimum and maximum viscosities are reported in each plot and the color scales are adapted to depict the logarithm of viscosity.

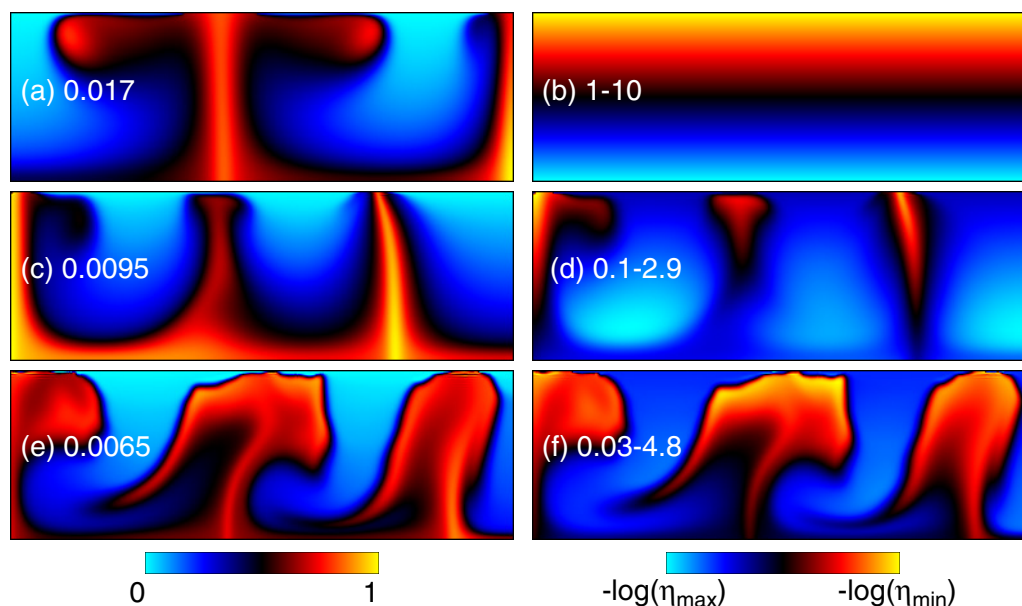


**Figure 8.** Snapshots of (left) temperature and (right) viscosity in a convecting box heated from within ( $Ra_i = 5 \times 10^6$  and  $R = 100$ ). The viscosity increases with depth by a factor 10 and varies exponentially with temperature. In the left column, the color table is between 0 and the maximum temperature  $T_{max}$  reported in each plot. In the right column, the color table is adapted to represent the viscosity variations between the minimum and maximum viscosities reported in each plot.

temperature are not drastically affected by the viscosity dependence on temperature. Therefore, we expect that the change in the convection pattern observed in the case of a constant viscosity (Figure 2) should occur with a temperature and depth-dependent viscosity, at least in the rather modest range of viscosity variations considered here ( $\approx 4$  orders of magnitude).

In the case of internal heating, a few cases with viscosity variations are shown in Figure 8. The same value is used for the internal Rayleigh number,  $Ra_i = 5 \times 10^6$  and the resistance is  $R = 100$ . The viscosity has the form  $\eta = \eta_0 \exp(c_1 z - c_2 T)$  with  $c_2 = 0, 250$  and  $1000$ , respectively, from top to bottom. The increase of viscosity with depth at constant temperature remains by a factor 10. In the case of internal heating the maximum temperature and the minimum and maximum viscosities are outputs of the computation. The maximum temperature and the minimum and maximum viscosities are indicated on each plot. Even with  $c_2 = 1000$  we only reach viscosity variations by a factor  $\approx 200$ , (f), as increasing  $c_2$  increases the effective Rayleigh number and decreases the temperature in agreement with Figure 6. Figure 6a, which shows a case where the viscosity is only depth dependent (see Figure 6b), corresponds to a case where the convection is rather “open” and where hot plumes are formed in the absence of bottom heating. The temperature dependence of the viscosity seems to increase the presence of hot plumes (Figure 6c) associated with low viscosity channels (Figure 6d). In the bottom row the large viscosity variations are mostly controlled by temperature, the convection pattern is very time dependent, but the presence of hot plumes is maintained.

Although this study of lateral viscosity variations with various resistance number is far from exhaustive, it seems that the transition from usual convection to a heat-pipe system occurs systematically mostly in basal heating convection but also with internal heating when the surface resistance is very low. With basal or internal heating, the opening of the surface leads to much lower internal temperatures.

## 6. Discussion

### 6.1. Cooling Rate of Young Planets

The cooling rate of a young planet neglecting radioactivity can be quantitatively assessed when noticing that minus the cooling rate  $-\rho C_p \partial T / \partial t$  (secular cooling) plays the same role as the radioactive source  $\rho P$  in the steady state heat equation [Krishnamurti, 1968]. The last major forming event of the Earth was likely the giant impact that formed the Moon [Canup and Asphaug, 2001; Canup, 2012; Cuk

and Stewart, 2012] which could have resulted in a large scale magma ocean. The cooling rate of this magma ocean is likely to be fast, because of the very high surface heat flow dominated by radiation, with values possibly around  $100 \text{ W m}^{-2}$  [Zahnle et al., 1988], that is  $10^3$  times larger than the present-day value. Even taking into account the larger concentration of radioactive elements in the early Earth, radiogenic heating from long-lived isotopes was negligible. Moreover, the formation of large planets is a protracted process and short-lived heat producing isotopes  $^{26}\text{Al}$  and  $^{60}\text{Fe}$  are likely extinct during the last stage of magma ocean crystallization. Therefore, let consider here the situation where secular cooling is the only energy source to drive convection. Sotin and Labrosse [1999] showed how a scaling for the average temperature in internally heated convection can be used to obtain an equation for the evolution of the average temperature in a planetary mantle. We follow the same approach here. The scaling of the average temperature (32) or (35) written in a general form is

$$\bar{T} = \frac{\rho P H^2}{2k} \theta = a \frac{\rho P H^2}{2k} \left( \frac{\alpha \rho^2 g P H^5}{\eta \kappa k} \right)^{-\beta}, \quad (36)$$

with  $\beta=1/2$  for an “open” boundary condition and  $\beta=1/4$  for a “closed” boundary condition. Substituting  $P$  by  $-C_p d\bar{T}/dt$  leads to an evolution equation for the average temperature,

$$\frac{d\bar{T}}{dt} = - \left( \frac{2\kappa}{aH^2} \right)^{1/(1-\beta)} \left( \frac{\alpha \rho g H^5}{\eta \kappa^2} \right)^{\beta/(1-\beta)} \bar{T}^{1/(1-\beta)}, \quad (37)$$

which can be used to model the thermal evolution of young planets. Introducing the initial temperature  $T_0$  and Rayleigh number  $Ra_0 = \rho g \alpha T_0 H^3 / (\kappa \eta)$ , and using the values of scaling factor obtained in both “closed” ( $a = 2.98$ ) and “open” ( $a = 5.7$ ) cases one gets

$$\left. \frac{d\bar{T}}{dt} \right|_c = -0.59 \frac{\kappa}{H} \left( \frac{\rho g \alpha}{\eta \kappa} \right)^{1/3} \bar{T}^{4/3} = -0.59 \frac{\kappa}{H^2} Ra_0^{1/3} \frac{\bar{T}^{4/3}}{\bar{T}_0^{1/3}} \quad (38)$$

$$\left. \frac{d\bar{T}}{dt} \right|_o = -0.12 \left( \frac{\rho g \alpha H}{\eta} \right) \bar{T}^2 = -0.12 \frac{\kappa}{H^2} Ra_0 \frac{\bar{T}^2}{T_0} \quad (39)$$

for the “closed” and “open” boundary conditions, respectively. Note that in the “open” case, where heat is not transported by diffusion, the cooling rate becomes effectively independent of the thermal diffusivity (the first equality in (39) does not contain  $\kappa$ ).

Equations (38) and (39) can be used to infer a typical cooling time scale, which are totally different with “closed” and “open” boundary conditions. In the “closed” case, a typical time of order  $\tau_c \simeq 1.7(H^2/\kappa)Ra_0^{-1/3}$  is expected, whereas in the “open” case we get  $\tau_o \simeq 8.3(H^2/\kappa)Ra_0^{-1}$ . In a young planet, the Rayleigh number is so large that the cooling rate is orders of magnitude faster in the “open” case than in the “closed” case.

## 6.2. Temperature and Convection Pattern of Very Active Planets

As already stressed by O’Reilly and Davies [1981] and Monnereau and Dubuffet [2002], planets in which heat might be advected through the surface by isolated vents offer the possibility to maintain at the same time a lithosphere, cold and thick on average, together with a very large heat flow delivered at the surface. This could be the case on Io, a Jovian moon where a huge heat flow (100 TW) is delivered by volcanoes lying on top of a thick elastic lithosphere [Carr et al., 1998], although the convection patterns of Figures 2 and 5 are not specifically intended to simulate the specificities of this moon [see e.g., Shahnas et al., 2013].

A heat-pipe mechanism can be a very efficient way to cool a young planet. It may have been the framework of convection on Earth before the onset of plate tectonics [Moore and Webb, 2013]. The extraction of heat by magmatic pipes deeply affects the convection pattern of the mantle (see Figure 2) as was already discussed by Monnereau and Dubuffet [2002] in the case of zero topographic resistance.

For a mantle heated from below, heat is transported from the bottom to the surface through heat pipes. This could occur after the core formation if the core was formed at high temperature [Monteux et al., 2009]. Even in the case of a mantle heated from within and simply cooled from the surface, heat pipes form (see Figure 5) when the topographic resistance is very low.

### 6.3. Present Day Convection of Earth's Mantle

In active regions with intense erosion with typical erosional diffusivity  $D_e = 10^{-3} \text{ m}^2 \text{ s}^{-1}$  [Flemings and Jordan, 1989], the resistance number of the Earth is only around  $R = 10^6$ , close to the value or  $Ra/10$  or  $Ra/100$  that we considered as the threshold for surface opening. This means that the heat flow ( $Nu - Ra$  relation) or the internal temperature should already be affected by the surface erosion of our planet. The extracted heat flow should be larger than what is predicted by "closed" convection models and the internal temperature should be lower. This confirms the effect of surface erosion on mantle dynamics already pointed out on a more regional scale [e.g., Avouac and Burov, 1996].

### 6.4. Inner Core Convection

The situation at the interface of the fluid core and solid inner core is somewhat akin to that at the surface. The topography that might be associated with the inner core dynamics is affected by the fluid core dynamics and the general cooling of the core. Fusion and solidification on the inner core surface change the topography associated with the inner core dynamics. Although the boundary conditions that we have derived are not adapted to this case, it has been suggested that the material velocity at the inner core surface may not be zero. This "open" condition may even allow the translation of the inner core, with solidification on one hemisphere and melting on the opposite hemisphere [Monnereau et al., 2010; Alboussière et al., 2010].

## 7. Conclusion

The dynamics of the surface of a planet may be much faster than its internal dynamics. A fast lateral transport at the surface due to erosion or to magma spreading extracts heat much more efficiently than the usually considered thermal diffusion across the lithosphere. A heat-pipe pattern may result, with hot plumes flowing through a cold lithosphere directly to the surface. In this situation, the lithosphere thickens and slowly sinks back to the mantle under the weight of the deposited material. This heat-pipe mechanism occurs in the case of a planet mantle heated from below but also in the case of a mantle heated from within if the topographic resistance is very low. In the case of a mantle simply cooling from its surface, the cooling rate is drastically increased.

In the present Earth, the heat carried out by magmatism is negligible. Even the huge Deccan traps with a volume of  $3 \times 10^{15} \text{ m}^3$  deposited in 1 Myr  $\sim$  65 Myr ago, only contributed by around 0.5 TW to Earth's energy budget [Courillot et al., 1986]. One needs therefore something like 80 times the volcanism of the Deccan Traps to carry out as much heat as what the Earth is presently losing by lithospheric conduction [Jaupart et al., 2007]. If this form of convection happened in the young Earth [Moore and Webb, 2013], our planet underwent a drastic dynamical change when it started to cool only by diffusion through a thick lithosphere.

The present erosion rate is likely larger than  $\Phi = 20 \times 10^9 \text{ kg yr}^{-1}$  which is the sediment load carried by a compilation of the largest rivers [Ludwig and Probst, 1998]. Notice that is  $\approx 5$  times larger than the annual magma mass that was brought to the surface during the Deccan traps event. At steady state, this erosion velocity  $v_e$  brings all the isotherms closer to the surface and therefore carries a heat flow of order  $\Phi C_p T$  where  $T$  is a typical asthenospheric temperature. Erosion should thus account for a heat flux of around 2 TW (4% of the heat budget). By far most of the sediments originate from the young orogenic belts in convergence area, mainly due to a combination of steep morphologies and high runoff intensities. This localized mass removal should also affect mantle convection on the large scale. This impact was even larger in the past when the Rayleigh number of the Earth was larger. At any rate, the relation between surface dynamics and internal processes might be more complex than what is usually thought.

### Acknowledgments

We thank Boris Kaus and Marc Monnereau for their constructive and very helpful comments. This work has been supported by the ANR CMBmelt 10-BLAN-622.

### References

- Alboussière, T., R. Deguen, and M. Melzani (2010), Melting-induced stratification above the Earth's inner core due to convective translation, *Nature*, 466 (7307), 744–747.
- Armitage, J. J., R. A. Duller, A. C. Whittaker, and P. A. Allen (2011), Transformation of tectonic and climatic signals from source to sedimentary archive, *Nat. Geosci.*, 4(4), 231–235.
- Avouac, J. P., and E. B. Burov (1996), Erosion as a driving mechanism of intracontinental mountain growth, *J. Geophys. Res.*, 101, 17,747–17,769.
- Biot, M., and H. Odé (1965), Theory of gravity instability with variable overburden and compaction, *Geophysics*, 30(2), 213–227.
- Canup, R., and E. Asphaug (2001), Origin of the Moon in a giant impact near the end of the Earth's formation, *Nature*, 412(6848), 708–712.
- Canup, R. M. (2012), Forming a Moon with an Earth-like composition via a giant impact, *Science*, 338(6110), 1052–1055.

- Carlson, R. W., and G. W. Langmuir (2000), Timescales of planetesimal formation and differentiation based on extinct and extant radioisotopes, in *Origin of the Earth and Moon*, edited by R. M. Canup and K. Righter, pp. 25–44, Univ. of Ariz. Press, Tucson.
- Carr, M., A. McEwen, K. Howard, F. Chuang, P. Thomas, P. Schuster, J. Oberst, G. Neukum, G. Schubert, and G. I. Team (1998), Mountains and calderas on Io: Possible implications for lithosphere structure and magma generation, *Icarus*, *135*(1), 146–165.
- Chemenda, A., M. Mattauer, J. Malavieille, and A. Bokun (1995), A mechanism for syn-collisional rock exhumation and associated normal faulting—Results from physical modeling, *Earth Planet. Sci. Lett.*, *132*(1–4), 225–232.
- Courtillot, V., J. Besse, D. Vandamme, R. Montigny, J. Jaeger, and H. Cappetta (1986), Deccan flood basalts at the Cretaceous tertiary boundary, *Earth Planet. Sci. Lett.*, *80*(3–4), 361–374.
- Cramer, F., H. Schmeling, G. J. Golabek, T. Duretz, R. Orendt, S. J. H. Buitert, D. A. May, B. J. P. Kaus, T. V. Gerya, and P. J. Tackley (2012a), A comparison of numerical surface topography calculations in geodynamic modelling: An evaluation of the ‘sticky air’ method, *Geophys. J. Int.*, *189*(1), 38–54.
- Cramer, F., P. J. Tackley, I. Meilick, T. V. Gerya, and B. J. P. Kaus (2012b), A free plate surface and weak oceanic crust produce single-sided subduction on Earth, *Geophys. Res. Lett.*, *39*, L03306, doi:10.1029/2011GL050046.
- Cuk, M., and S. T. Stewart (2012), Making the Moon from a fast-spinning Earth: A giant impact followed by resonant despinning, *Science*, *338*(6110), 1047–1052.
- Culling, W. (1963), Soil creep and the development of hillside slopes, *J. Geol.*, *71*, 127–161.
- Dadson, S., et al. (2003), Links between erosion, runoff variability and seismicity in the Taiwan orogen, *Nature*, *426*(6967), 648–651.
- Dubuffet, F., M. Rabinowicz, and M. Monnereau (2000), Multiple scales in mantle convection, *Earth Planet. Sci. Lett.*, *178*, 351–366.
- Duretz, T., D. A. May, T. V. Gerya, and P. J. Tackley (2011), Discretization errors and free surface stabilization in the finite difference and marker-in-cell method for applied geodynamics: A numerical study, *Geochem. Geophys. Geosyst.*, *12*, Q07004, doi:10.1029/2011GC003567.
- Fernandes, N. F., and W. E. Dietrich (1997), Hillslope evolution by diffusive processes: The time scale for equilibrium adjustments, *Water Resour. Res.*, *33*, 1307–1318.
- Flemings, P. B., and T. E. Jordan (1989), A synthetic stratigraphic model of foreland basin development, *J. Geophys. Res.*, *94*, 3851–3866.
- Gerya, T., and B. Stöckhert (2006), Two-dimensional numerical modeling of tectonic and metamorphic histories at active continental margins, *Int. J. Earth Sci.*, *95*(2), 250–274.
- Huppert, H. (1982), The propagation of two-dimensional and axisymmetric viscous gravity currents over a rigid horizontal surface, *J. Fluid Mech.*, *121*, 43–58.
- Iaffaldano, G., L. Husson, and H.-P. Bunge (2011), Monsoon speeds up Indian plate motion, *Earth Planet. Sci. Lett.*, *304*(3–4), 503–510.
- Jaupart, C., S. Labrosse, and J.-C. Mareschal (2007), 7.06—Temperatures, heat and energy in the mantle of the earth, in *Treatise on Geophysics*, edited by G. Schubert, pp. 253–303, Elsevier, Amsterdam.
- Kaus, B. J. P., and T. W. Becker (2007), Effects of elasticity on the Rayleigh-Taylor instability: Implications for large-scale geodynamics, *Geophys. J. Int.*, *168*(2), 843–862.
- Kaus, B. J. P., C. Steedman, and T. W. Becker (2008), From passive continental margin to mountain belt: Insights from analytical and numerical models and application to Taiwan, *Earth Planet. Sci. Lett.*, *171*(1–4, SI), 235–251.
- Kaus, B. J. P., H. Mühlhaus, and D. A. May (2010), A stabilization algorithm for geodynamic numerical simulations with a free surface, *Phys. Earth Planet. Inter.*, *181*, 12–20.
- Kirkby, M. J. (1971), Hillslope process-response models based on the continuity equation, *Inst. Br. Geogr. Spec. Publ.*, *3*, 15–30.
- Krishnamurti, R. (1968), Finite amplitude convection with changing mean temperature. Part 1. Theory, *J. Fluid Mech.*, *33*, 445–455.
- Ludwig, W., and J. Probst (1998), River sediment discharge to the oceans: Present-day controls and global budgets, *Am. J. Sci.*, *298*(4), 265–295.
- Monnereau, M., and F. Dubuffet (2002), Is Io’s mantle really molten?, *Icarus*, *158*, 450–459.
- Monnereau, M., M. Calvet, L. Margerin, and A. Souriau (2010), Lopsided growth of Earth’s inner core, *Science*, *328*(5981), 1014–1017.
- Monteux, J., Y. Ricard, N. Coltice, F. Dubuffet, and M. Ulvrova (2009), A model of metal-silicate separation on growing planets, *Earth Planet. Sci. Lett.*, *287*(3–4), 353–362.
- Moore, W., and A. Webb (2013), Heat-pipe Earth, *Nature*, *501*, 501–505.
- O’Reilly, T., and G. Davies (1981), Magma transport of heat on Io—A mechanism allowing a thick lithosphere, *Geophys. Res. Lett.*, *8*, 313–316.
- Parmentier, E. M., C. Sotin, and B. J. Travis (1994), Turbulent 3-D thermal convection in an infinite Prandtl number, volumetrically heated fluid: Implications for mantle dynamics, *Geophys. J. Int.*, *116*, 241–251.
- Peaceman, D. W., and H. H. Rachford (1955), The numerical solution of parabolic and elliptic differential equations, *J. Soc. Ind. Appl. Math.*, *3*(1), 28–41.
- Peale, S., P. Cassen, and R. Reynold (1979), Melting of Io by tidal dissipation, *Science*, *203*(4383), 892–894.
- Ricard, Y. (2007), Physics of mantle convection, in *Mantle Dynamics, Vol. 7 of Treatise on Geophysics*, edited by S. Gerald, and D. Bercovici, chap. 7.02, pp. 31–87, Elsevier Sci., N. Y.
- Ricard, Y., O. Šrámek, and F. Dubuffet (2009), A multi-phase model of runaway core-mantle segregation in planetary embryos, *Earth Planet. Sci. Lett.*, *284*(1–2), 144–150.
- Richards, M. A., and B. H. Hager (1984), Geoid anomalies in a dynamic Earth, *J. Geophys. Res.*, *89*, 5987–6002.
- Robuchon, G., G. Choblet, G. Tobie, O. Čadež, C. Sotin, and O. Grasset (2010), Coupling of thermal evolution and despinning of early Iapetus, *Icarus*, *207*(2), 959–971.
- Schmeling, H., et al. (2008), A benchmark comparison of spontaneous subduction models—Towards a free surface, *Phys. Earth Planet. Inter.*, *171*, 198–223.
- Schubert, G., D. L. Turcotte, and P. Olson (2001), *Mantle Convection in the Earth and Planets*, 940 pp., Cambridge Univ. Press, Cambridge, U. K.
- Shahnas, M. H., R. N. Pysklywec, and W. R. Peltier (2013), Layered convection in Io: Implications for short-wavelength surface topography and heat flow, *Icarus*, *225*(1), 15–27.
- Sotin, C., and S. Labrosse (1999), Three-dimensional thermal convection of an isoviscous, infinite-Prandtl-number fluid heated from within and from below: Applications to heat transfer in planetary mantles, *Phys. Earth Planet. Inter.*, *112*(3–4), 171–190.
- Tonks, W., and H. Melosh (1993), Magma ocean formation due to giant impacts, *J. Geophys. Res.*, *98*, 5319–5333.
- Turcotte, D. (1989), A heat pipe mechanism for volcanism and tectonics on Venus, *J. Geophys. Res.*, *94*, 2779–2785.
- Turcotte, D. L., and G. Schubert (1982), *Geodynamics: Applications of Continuum Physics to Geological Problems*, John Wiley, N. Y.
- Šrámek, O., Y. Ricard, and F. Dubuffet (2010), A multiphase model of core formation, *Geophys. J. Int.*, *181*(1), 198–220.
- Zahnle, K. J., J. F. Kasting, and J. B. Pollack (1988), Evolution of a steam atmosphere during Earth’s accretion, *Icarus*, *74*(1), 62–97.
- Zhong, S. J., M. Gurnis, and L. Moresi (1996), Free surface formulation of mantle convection, part 1: Basic theory and implication to plumes, *Geophys. J. Int.*, *127*, 708–718.